ELSEVIER

PII: S0032-3861(96)00930-5

Polymer Vol. 38 No. 14, pp. 3581–3589, 1997

0032-3861/97/$17.00 + 0.00

Plasma treatment of polyolefins: Influence of material composition: 1. Bulk and surface characterization

Anna Nihlstrand and Thomas Hjertberg*
Department of Polymer Technology, Chalmers University of Technology, S-412 96 Gothenburg, Sweden

and Kenth Johansson
Institute for Surface Chemistry, Box 5607, S-114 86 Stockholm, Sweden
(Received 19 August 1996)

Injection-moulded plates of ten polypropylene (PP) and thermoplastic polyolefin (TPO) materials with varying material composition (different type of rubber, varying degree of ethylene etc.) were characterized before and after oxygen plasma treatments. Untreated materials were studied by means of differential scanning calorimetry (d.s.c.), size exclusion chromatography (s.e.c.), Fourier-transform infrared spectroscopy (*FT*i.r.), attenuated total reflectance (ATR) and transmission measurements, and the effect of plasma treatment conditions was followed by X-ray photoelectron spectroscopy (X.p.s.) and contact angle measurements. S.e.c. analysis revealed only minor variations among the materials, while the d.s.c. and *FT*i.r. experiments confirmed that the differences were to be expected as a result of the variation in material composition. The *FT*i.r.–ATR results showed that all samples had a gradient in material composition. The materials were generally more rich in PP in the topmost ~200 nm than in the first ~800 nm, and a lesser extent of ethylene modification and/or rubber was observed in the topmost ~200 nm. It was also shown that the degree of surface crystallinity was normally greater at ~800 nm than at ~200 nm, and that a higher mould temperature led to a higher degree of surface crystallinity. The water contact angles and the atomic composition showed that the materials were more oxidized after plasma treatment at high power-to-gas pressure (P/G) ratios than at low ratios. Moreover, the dependence on material composition was weak for samples that were plasma-treated at low P/G ratios whereas the materials that were least ethylene-modified were less oxidized than the others at high P/G ratios. © 1997 Elsevier Science Ltd.

(Keywords: oxygen plasma treatment; characterization; material composition)

INTRODUCTION

Polypropylene (PP) and physical blends of PP with ethylene-propylene rubber (EPR) or ethylene-propylene-diene-monomer (EPDM) rubber (also known as thermoplastic polyolefins, TPOs) are widely used materials in industrial applications. One important area is the automotive industry, in which they are used for manufacturing exterior and interior components. The low surface energy is a major drawback, however, as components such as bumpers and dashboards must often be lacquered or glued to fulfil application demands. Achieving satisfactory adhesion properties thus requires a pretreatment that can promote bondability. A commonly used pretreatment specifically for the successful lacquering of bumpers, has involved the use of an adhesion promoter, i.e. a chlorinated polyolefin dissolved in a mixture of organic solvents such as toluene and xylene[1]. Although solvent-based primers work satisfactorily from an adhesion point of view, their use is complicated by the fact that both chlorinated products and organic solvents are undesirable from an environmental point of view.

Surface modification by cold-glow discharge plasmas is an environmentally attractive alternative to the use of primers. A low-temperature plasma is a partially ionized gas consisting of atoms, molecules, ions, radicals and a multitude of excited species[2]. A broad spectrum of electromagnetic radiation is also produced as the excited species return to lower energy states[3]. Oxygen and nitrogen are gases commonly used for the plasma treatment of polyolefins. These result in oxidation of the surface and hence an increased surface energy. In our experience, it is rarely the degree of oxidation that determines the subsequent level of adhesion, but rather the plasma parameters[4] and the material composition[5]. The plasma parameters mainly affect the concentration of active species in the plasma[6]—in particular the radiation intensity—and thus the *amount* of radicals being formed in the substrate, while the material composition chiefly determines what *types* of radicals are formed. Consequently, as TPOs do not form an unequivocally defined group of materials (although they are chemically similar), their response towards plasma treatments are completely different[5,7].

* To whom correspondence should be addressed

The *primary* goal of this study, which is the first part of two, was to characterize a number of specifically designed PP matrices and TPO materials and to carefully analyse their surface properties before and after selected oxygen plasma treatments. The purpose was to elucidate whether the materials respond differently towards oxygen plasma treatments as a result of their chemical and morphological composition. The *ultimate* goal, however, was to determine whether a relation could be found that correlates the material composition with the adhesion properties obtained after plasma treatments. The adhesion properties and the locus of failure will be discussed in part two[7].

EXPERIMENTAL

Materials

Ten polypropylene-based materials supplied by Boreralis, Norway, were used in this study. The materials, designated A1–A4 and B1–B6, were specifically designed for this study and are presented in *Table 1*. Materials A1–A4 are 'PPs' with a varying degree and type of ethylene modification while materials B1–B6 are TPOs. All TPOs contain the same amount of rubber (25 wt%). This set of materials allows us to compare and investigate the effect of the following parameters:

(a) random *versus* block ethylene modification;
(b) increasing amount of ethylene modification;
(c) choice of matrix (same rubber);
(d) choice of rubber (same matrix);
(e) molecular weight of rubber phase (same type);
(f) mould temperature (i.e. surface crystallinity).

The materials contain comparable (standard) amounts of stabilizers and, in addition, all materials except for A1 contain a small amount of carbon black. The materials were received as injection-moulded plates of the size 150 × 70 mm and a thickness of 3 mm. All materials were injection-moulded using the same processing parameters (mould temperature 40°C and melt temperature 230°C) except for B6, which was injection-moulded into plates using mould temperatures of 30°C and 70°C. Finally, it should be noted that, although the material compositions are known, these materials are still based on commercial components, one consequence of which was that we did not have access to the pure rubbers.

Differential scanning calorimetry (d.s.c.)

D.s.c. was used to obtain information on the melting temperature (T_m), crystallization temperature (T_c) and melting enthalpy of the bulk materials. In order to more easily compare the materials, the melting enthalphies were recalculated as the degree of crystallinity (C) by using 165 J g^{-1} as the reference heat of fusion for a 100% crystalline isotactic PP[8]. The samples were exposed to the following temperature ramp: heating 40–200°C; cooling 200–40°C; heating 40–200°C. All runs were performed at a temperature rate of 10°C min^{-1}, and typical sample weights were 10 mg. The measurements were carried out using a DSC 7 from Perkin–Elmer. The reported values for T_m and C are calculated from the second heating run.

Size exclusion chromatography (s.e.c.)

Molecular weights (M_W) of the materials were obtained by s.e.c.. The samples were dissolved in 1,2,4-trichlorobenzene (5 g l^{-1}) at 135°C for 7 h. The measurements were carried out on a Waters 150 CV system equipped with three columns—two Shodex AT-80 M/S and one MP 613 E column (particle size 10 μm, normal pore size distribution)—swollen in 1,2,4-trichlorobenzene. The calibration is based on narrow polystyrene (PS) standards and transferred to polyethylene (PE) via universal calibration. The molecular weights were then recalculated to PP calibration.

Fourier-transform infrared spectroscopy (FTi.r.)

*FT*i.r. spectroscopy was used to obtain structural information on the materials. For analysis of the bulk

Table 1 Description and chemical composition of materials

Designation	Material	Description	C2 content[a] (mol%)	Diene content (mol%)
A1	'PP'	Randomly C2-modified PP	9	–
A2	'PP'	Block C2-modified PP	9	–
A3	'PP'	Block C2-modified PP	20	–
A4	'PP'	Block C2-modified PP	33	–
B1	TPO	Randomly C2-modified PP (same as A1)	9	–
		+25 wt% EPR	64	–
B2	TPO	Block C2-modified PP (same as A3)	20	–
		+25 wt% EPR	64	–
B3	TPO	Randomly diene-modified PP	–	1.4
		+25 wt% EPR	64	–
B4	TPO	Block C2-modified PP (same as A3)	20	–
		+25 wt% EPDM	63	1.3
B5	TPO	Randomly diene-modified PP	–	1.4
		+25 wt% EPDM	63	1.3
B6[b]	TPO	Block C2-modified PP (same as A3)	20	–
		+25 wt% EPR[c]	64	–

[a] C2 is the ethylene content
[b] Plates were produced using two different mould temperatures: 30°C (B6^1) and 70°C (B6^2)
[c] The EPR in B6 has a higher molecular weight than the EPR in materials B1–B3

materials, thin films (~40–50 μm) were made by melt-pressing (190°C, 5 tons, 30 s) small pieces cut from the plates. The films were analysed by ordinary transmission measurements. Attenuated total reflectance (ATR) was used for analysis of surfaces. ATR is the *FT*i.r. technique normally used for surface characterization of polymers, and the penetration depth varies between 0.1 and 10 μm depending on wavelength (λ), angle of incidence (θ), refractive index of the crystal (n_c) and the refractive index of the sample (n_s)[9].

Two different crystals were used in this study: germanium (Ge), $n_c = 4.0$; and KRS-5 (a mixture of thallium bromide and thallium iodide), $n_c = 2.35$. The incident angle was 48.7° when the Ge crystal was used (crystal endface angle 45°; optics angle 60°) and 45° when the KRS-5 crystal was used (crystal endface angle 45°, optics angle 45°)[10]. The refractive index of the polymer samples is considered to be similar to a PP homopolymer, i.e. $n_s = 1.5$[10]. Using these conditions, the penetration depth (d_p) is approximately 0.06 λ for the Ge crystal and 0.22 λ for the KRS-5 crystal. The sample chamber was purged with dried air to achieve high quality spectra. 20 scans were co-added for all samples, and the resolution was 4 cm^{-1}. The analyses were carried out on a Perkin–Elmer FTIR 2000 system equipped with a triglycine sulfate (TGS) detector.

Plasma treatments

The plasma reactor used in this study is a commercially available batch reactor (Technics Plasma, model 3027-E) located at the Institute for Surface Chemistry, Stockholm. The process chamber is made of aluminium and its inner dimensions (width × height × depth) are 650 × 600 × 700 mm. The chamber, originally designed for chemical etching of printed circuit boards, contains 120 tubular electrodes, eight gas inlets and two gas channels with flow regulators. The power generator (ENI, model EGR 3200B) is tuned at 35 kHz, with a maximum output of up to 3000 W. The vacuum system includes a two-stage monoblock pump (Leybold-Heraeus, model DK 100) with an ultimate pressure of 15–20 mTorr and a working pressure in the range of 100–1200 mTorr. The pressure in the chamber is controlled by a Leybold-Heraeus Thermovac TC gauge and a MKS Baratron capacitance manometer (Type 221A, Power Supply/Digital readout model PDR-C-1B).

Prior to treatments, the system was purged in order to remove impurities and to achieve as reproducible treatment conditions as possible. The purging procedure included evacuation of the system down to 60 mTorr, inlet of oxygen to a pressure of 1000 mTorr and a second evacuation of the system down to 60 mTorr. This cycle was repeated twice before the pressure was raised to the desired treatment pressure. The reactor was purged with oxygen for 1 min before the plasma was ignited. Treatments were carried out at different discharge powers (200–2000 W), combined with various gas pressures (100–800 mTorr), resulting in power-to-gas pressure (P/G) ratios between 0.25 and 20, see *Table 2*. No measurement was made of the flow rate. The treatment time in all experiments was 30 s. Six plates were treated each time, and the sample plates were symmetrically placed at fixed positions in the upper part of the reactor.

Static contact angle measurements

Static contact angle measurements using water as the probing liquid were carried out on both untreated and plasma-treated samples in order to follow the changes in wettability. Droplets of deionized water (4 μl in volume) were positioned at different locations on the plates and at least six readings were taken for each plate in order to determine average values. Both the advancing and the receding contact angles were measured. The measurements were made immediately before lacquering, and typical standard deviations were 2–3°.

Table 2 Power-to-gas pressure (P/G) ratios resolved into powers and gas pressures

P/G (W mTorr^{-1})	Power (W)	Gas pressure (mTorr)	Materials treated
0.25	200	800	A1–A4 and B1–B6
1.0	800	800	A1–A4
2.5	2000	800	A1–A4 and B1–B6
8.0	800	100	A1–A4
10	2000	200	B1–B6
20	2000	100	B1–B6

X-ray photoelectron spectroscopy (X.p.s.)

X.p.s. was used to determine the atomic composition of untreated and plasma-treated samples. The analyses were carried out using a Mg K_α X-ray source (1253.6 eV) at 11 kV and 250 W. The pressure during acquisition was $< 1 \times 10^{-9}$ Torr and the take-off angle (the angle between the analyzer and the sample surface), ϕ, was varied between 25° and 70°, corresponding to an 'effective' sampling depth of *ca.* 4–9.5 nm[11]. The analysed area was 0.8 mm in diameter. The analyses were performed on a PHI 5500 ESCA system from Perkin–Elmer, and the sensitivity factors used were according to the Perkin Elmer manual. The X.p.s. data are estimated to be accurate to within ± 1 atom%.

RESULTS AND DISCUSSION

Analysis of bulk materials

D.s.c. The numerical results of the d.s.c. and s.e.c. experiments are summarized in *Table 3*. The d.s.c. melting curves are shown in *Figure 1*. The block character of the ethylene modification and the increasing ethylene content in the series A2–A4 are evident in form of weak PE melting peaks in the region of 110–125°C (see *Figure 1*). Although the ethylene content varies, *Table 3* shows that no significant difference in the melting

Table 3 Melting temperature (T_m), degree of crystallinity (C), crystallization temperature (T_c), and molecular weights—number (M_n) and weight (M_w) averages—as measured by d.s.c. and s.e.c.. Molecular weights are given in PP calibration

Designation	T_m (°C)	C (%)	$T_{c,start}$ (°C)	$T_{c,peak}$ (°C)	$\bar{M}_n \times 10^{-3}$ (g mol^{-1})	$\bar{M}_w \times 10^{-3}$ (g mol^{-1})
A1	150	54	119	113	32.5	200
A2	163	56	124	112	31.5	200
A3	161	51	121	110	28.2	243
A4	160	37	122	111	26.0	220
B1	150	41	122	113	40.7	178
B2	163	39	132	118	27.4	190
B3[a]	146	34	118	105	35.9	244
B4	162	42	129	116	24.8	195
B5[a]	147	39	123	106	27.6	237
B6	162	34	123	113	34.5	196

[a] Corresponding values for the diene-modified PP used in these materials are 148°C, 49%, 121°C, 111°C, 37.4×10^3 g mol^{-1} and 280×10^3 g mol^{-1}

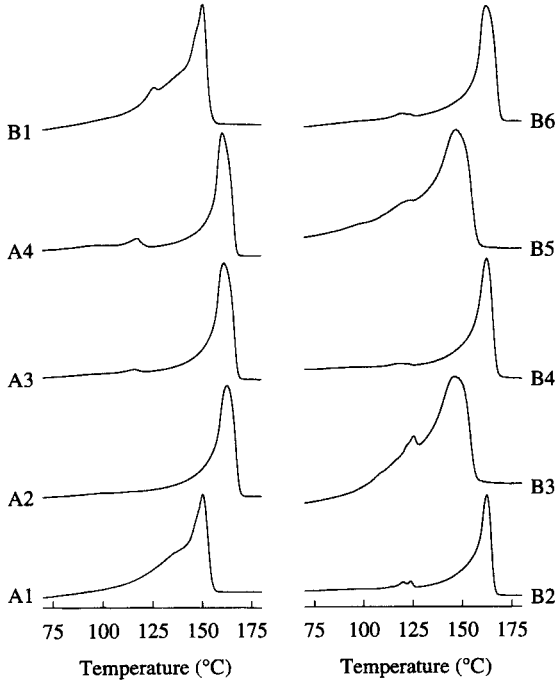

Figure 1 Melting curves of the materials as measured by d.s.c. Temperature rate 10°C min^{-1}

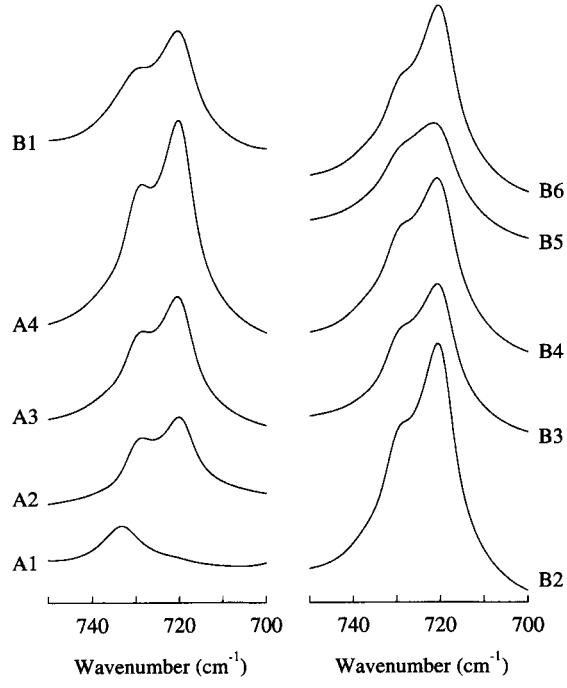

Figure 2 *FT*i.r. transmission spectra (in absorbance) for films of approximately the same thickness. The figure shows the $-CH_2-$ rocking vibration. A split peak indicates partial crystallinity

temperatures (T_m) can be observed except for the randomly modified PP, which reveals a lower T_m. Furthermore, materials B3 and B5 (based on the diene-modified PP) reveal a lower degree of crystallinity and a lower T_m than B2 and B4 (corresponding materials based on A3). Similar to A1, the former materials' decrease in T_m is a consequence of the PP matrix being randomly modified. Moreover, it can be deduced from *Table 3* that all TPOs have a degree of crystallinity close to that expected for these materials, i.e. 75% of the value obtained for the corresponding PP matrix. Comparing A3, B2 and B4 (pure block ethylene-modified PP matrix and corresponding materials with EPR and EPDM), and B3 with B5 (diene-modified PP with EPR and EPDM, respectively), it can be concluded that the ethylene in the EPR is to a higher extent than in the EPDM in the form of blocks. This is shown by larger peaks in the region where PE melts in the case of B2 and B3 as compared with B4 and B5. A comparison of A1 and B1 supports this conclusion. Similarly, a comparison of B2 with B6 reveals that the EPR with the higher molecular weight also has less ethylene in the form of blocks than the 'normal' EPR. With respect to the crystallization behaviour of the materials, the most interesting observation is that the rubber phase in B2 and B4 leads to a considerable increase in both the start and peak crystallization temperatures as compared with the pure matrix (A3), while the rubber phase in B3 and B5 instead lowers the peak crystallization temperature as compared with the PP diene matrix. This may affect the segregation and crystallization behaviour of the materials during production of the plates.

S.e.c. *Table 3* also reports the molecular weights of the materials in PP calibration (number and weight averages). It can be seen that the molecular weights are in the same order of magnitude, although materials B3 and B5 have slightly higher weight averages, owing to the fact that the matrix itself has a higher weight average (280×10^3 g mol^{-1}). It should also be noted that material A3 has a slightly higher weight average than the other PPs.

FT*i.r.* The interesting part of the *FT*i.r. transmission spectra is the peak in the region of 720–740 cm^{-1}, which corresponds to the $-CH_2-$ rocking vibration. This part of the spectra is shown in *Figure 2*. The spectra are shifted vertically but are otherwise comparable. The position of the peak gives an indication of how the ethylene units are distributed[12,13] and, as the films have approximately the same thickness, the peak intensity gives an estimate of the ethylene content. In addition, the shape of the peak provides information on the crystallinity of the sample—a single peak at ~ 720 cm^{-1} indicates no crystallinity, whereas a doublet with peaks around 720 and 730 cm^{-1} indicates partial crystallinity[12]. The figure confirms that the ethylene content increases from A2–A4 and that the major part of the ethylene units are present in long blocks. It is also evident that the ethylene in A1 is randomly distributed, as the peak is positioned at 733 cm^{-1}, corresponding to isolated ethylene units[13]. Moreover, the figure supports the d.s.c. results as it indicates a greater extent of ethylene to be in the form of blocks in the materials containing the 'normal' EPR (compare B2 with B4, and B3 with B5). This is further supported by difference spectra made between B2 and A3, and between B4 and A3, which showed that the EPR had much more material at 720 cm^{-1} than did the EPDM, which primarily had a peak at ~ 724 cm^{-1}, indicating shorter blocks[12]. Furthermore, the EPR in B6 also seems to have less ethylene in the form of blocks than the EPR in B2. In addition, the block character of the ethylene in the 'normal' EPR is illustrated by comparing A1 and B1; in B1, peaks appear at 720 and 730 cm^{-1} and, as no sign of these peaks is observed for A1, they must originate from the EPR.

Surface characterization of unmodified materials

FT*i.r.–ATR.* By using both Ge and KRS-5 crystals, *FT*i.r.–ATR can be used to compare the structural composition at different depths from the surface. When the Ge crystal is used, the topmost ~200 nm is analysed, while the first ~800 nm is analysed when using the KRS-5 crystal (the values are estimated for $\lambda = 2900\,cm^{-1}$). The *FT*i.r.–ATR spectra of the $-CH_3$ and $-CH_2-$ asymmetric (as) and symmetric (s) stretching region of the materials are shown in *Figures 3a–6b*. The spectra are scaled with respect to the peak at $2920\,cm^{-1}$, i.e. the $2920\,cm^{-1}$ peaks in all spectra have the same intensity. We have chosen to display the results in four different plots in order to more easily see and compare the influence of certain material parameters. As a result, some materials may be present in more than one plot. The peak intensities and peak positions in this part of the spectra provide useful information about the materials. The ratio between $2950\,cm^{-1}$ ($-CH_3$, as) and $2920\,cm^{-1}$ ($-CH_2-$, as) gives a measure of the extent of propylene and ethylene in the surface region. It is also possible to gain information on the surface crystallinity by studying the $-CH_3$ (as) peak. The band at $2959\,cm^{-1}$, which is often observed as a broadening of the band at $2950\,cm^{-1}$, becomes better resolved and less intense as the degree of crystallinity increases[14]. Another interesting part of the spectra is the $-CH_2-$ (s) stretching region between $2840–2850\,cm^{-1}$. If the peak appears at $2840\,cm^{-1}$, it corresponds to methylene units present in isotactic PP; if it instead appears at $2850\,cm^{-1}$, it corresponds to methylene units present in the rubber phase or in the ethylene-modified part of the PP[14,15]. However, a transmission spectrum of A1 showed no sign of a peak at $2850\,cm^{-1}$, which indicates that, if the ethylene units are isolated, these two methylene units also appear at $2840\,cm^{-1}$. Thus, the peak at $2850\,cm^{-1}$ indicates the presence of ethylene in the form of shorter or longer blocks.

Figure 3 displays the ATR spectra obtained for the different PPs using the KRS-5 crystal (a) and the Ge crystal (b). It is evident that more $-CH_3$ groups ($2950\,cm^{-1}$) are present in the first ~200 nm than in the first ~800 nm of the block ethylene-modified PPs (A2–A4), while the randomly modified PP (A1) shows roughly the same amount at both depths. Comparing the spectra obtained using the KRS-5 crystal, the most obvious difference among the materials is the peak at $2850\,cm^{-1}$ that arises from the ethylene modification, which increases from A2 to A4—as one would expect according to the bulk composition. Furthermore, the spectra obtained for A1 at the two depths reveal no differences. As the transmission spectrum for A1 revealed no peak at $2850\,cm^{-1}$, nothing can be concluded as regards the concentration of ethylene at the two depths for this material. This is not true for A2–A4, however, which show quite different compositions at the two depths. In fact, no sign of the block ethylene modification (absence of the peak at $2850\,cm^{-1}$) can be observed for A2, while a weak sign can be observed for A3 when the Ge crystal is used. For A4, the peak is clearly present, although it is less intense than in the case when the KRS-5 crystal is used.

Figure 4 compares the spectra obtained for TPOs that contain the same rubber (EPR) but which are based on different PP matrices. As for A2–A4, B2 and B3 show a

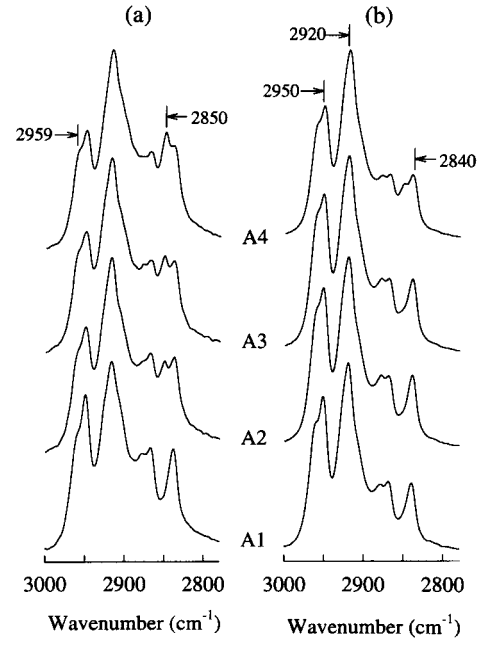

Figure 3 Comparison of *FT*i.r.–ATR spectra (in absorbance) of four differently modified PPs. (a) Spectra obtained using KRS-5. (b) Spectra obtained using Ge

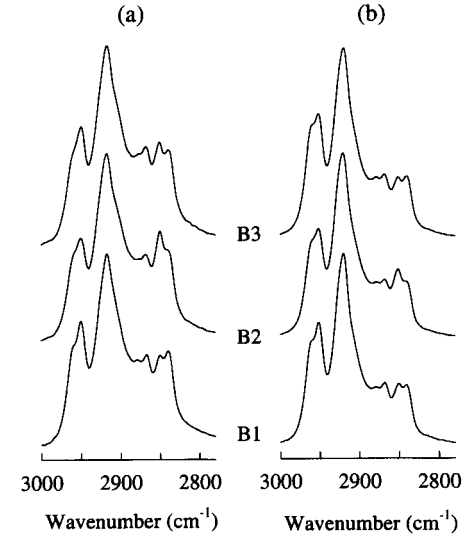

Figure 4 Comparison of *FT*i.r.–ATR spectra (in absorbance) of materials that contain the same rubber phase but are based on different matrices. (a) Spectra obtained using KRS-5. (b) Spectra obtained using Ge

greater peak at $2950\,cm^{-1}$ when the Ge crystal is used than when the KRS-5 crystal is used, while instead B1 shows a slightly higher $2950\,cm^{-1}$ peak at the KRS-5 depth. The figure also reveals that, at the KRS-5 depth, B2 is the material with the largest peak at $2850\,cm^{-1}$, followed by B3 and B1. In the case of B2, the peak may originate from the ethylene modification and/or from the rubber phase, whereas the peak must originate from the rubber in the case of B1 and B3. This is because, according to the transmission spectra, A1 does not reveal any peak at $2850\,cm^{-1}$, while the matrix is diene-modified in the case of B3 and consequently does not contain any ethylene. At the Ge depth, B2 is again the material with the largest peak at $2850\,cm^{-1}$, followed by

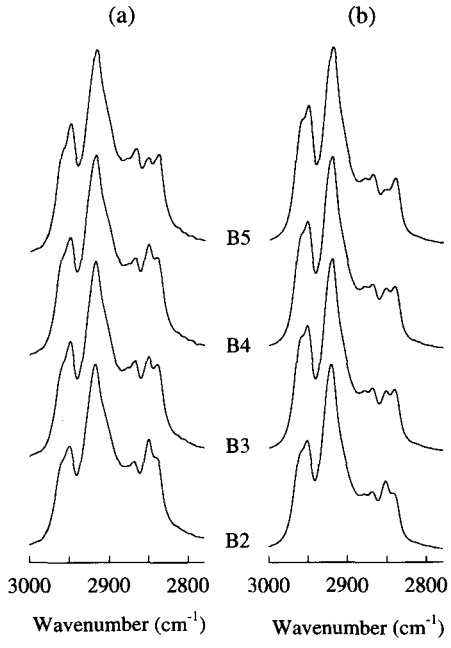

Figure 5 Comparison of *FT*i.r.–ATR spectra (in absorbance) of materials containing EPR (B2, B3) and EPDM (B4, B5) rubber. (a) Spectra obtained using KRS-5. (b) Spectra obtained using Ge

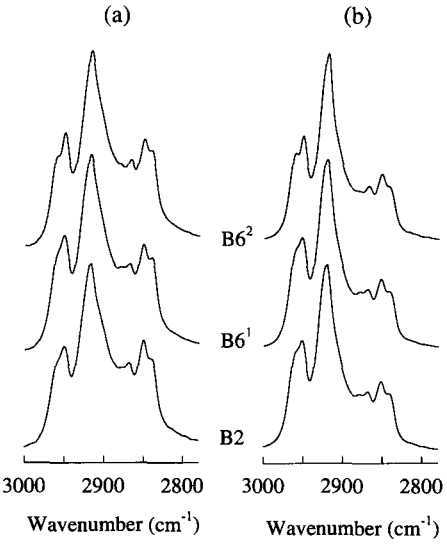

Figure 6 Comparison of *FT*i.r.–ATR spectra (in absorbance) of materials containing EPR rubber of different molecular weights. (a) Spectra obtained using KRS-5. (b) Spectra obtained using Ge

B1 and B3. In this case, however, it appears more likely that the peak originates from the rubber phase, as no sign of this peak is observed for A3 at this depth (*Figure 3b*). Moreover, it is interesting again to note that B1, contrary to all other materials, seems to have a lesser amount of rubber (more PP) at the KRS-5 depth than at the Ge depth, as the peak at 2850 cm^{-1} is smaller in the former case.

Figure 5 shows materials that are based on the same matrix (B2/B4 and B3/B5) but that contain different types of rubber, EPR (B2/B3) or EPDM (B4/B5). As for previous samples, a greater extent of $-CH_3$ and a lesser extent of rubber and/or ethylene-modified material is found at the Ge depth than at the KRS-5 depth. It can also be seen that the peak at 2850 cm^{-1} is greater for the materials containing EPR than for corresponding materials containing EPDM, in particular for the spectra shown in (b). This may be interpreted such that more EPR than EPDM is present in the first ~200 nm, or that a greater extent of ethylene in the form of blocks is present in this region for the materials containing the EPR (recall the d.s.c. melting curves and the *FT*i.r. transmission spectra).

Figure 6 displays materials based on the same matrix and rubber type (EPR) but with the difference that the rubbers have different molecular weights (M_W). The figure also shows the effect of a higher mould temperature during production of the plates. A higher mould temperature primarily affects the degree of surface crystallinity—the higher the mould temperature, the higher the crystallinity (the peak at 2959 cm^{-1} is better resolved in the case $B6^2$, i.e. mould temperature 70°C). The effect can be observed at both depths, but is less pronounced at the KRS-5 depth, although the degree of crystallinity for most of the samples is lower at the Ge depth than at the KRS-5 depth, at least as indicated by the 2959 cm^{-1} peak. Another interesting observation is that the rubber in $B6^1$ and $B6^2$ seems to be equally distributed at the two depths, which is not the case for B2 or any of the other TPOs. Still another observation is that all three samples appear to have a nearly identical composition down to a depth of ~200 nm, as they have similar 2950 cm^{-1}/2920 cm^{-1} ratios and rubber contents (2850 cm^{-1}).

It is obvious from the above discussion that the surface composition is a function of both analysing depth and material composition. A few general trends can be distinguished:

(a) the surface becomes more rich in PP (as measured by the 2950 cm^{-1}/2920 cm^{-1} ratio) when approaching the outermost surface, with the sole exception of B1;
(b) the extent of ethylene modification and/or rubber is higher at the KRS-5 depth than at the Ge depth (comparison of 2850 cm^{-1} and 2840 cm^{-1}), again with the exception of B1. This agrees with the increase in PP observed when approaching the surface;
(c) most samples show a lower degree of surface crystallinity (increase in amorphous material) when approaching the outermost surface.

Valence-band X.p.s. As the *FT*i.r.–ATR results indicated the extent of PP to increase when approaching the outermost surface, an attempt was made to gain structural information on a thinner layer than can be reached by *FT*i.r.–ATR. The X.p.s. technique—with a probing depth of less than 10 nm—is more surface-sensitive than *FT*i.r.–ATR but, although the core level lines give valuable information about the chemical composition, they provide little information on structure (similar spectra will be obtained for saturated hydrocarbon polymers). On the other hand, the valence-band (VB) region (~0–40 eV) can be used to identify hydrocarbon polymers, as each polymer has its own characteristic VB[16]. Thus, in favourable cases, the VB region can be used to distinguish whether it is mainly PP or rubber that is present at the outermost surface. Unfortunately, all materials display quite similar VB structures, although the TPOs generally show a lesser resemblance to the characteristic PP structure than do the PPs, as exemplified in *Figure 7*. This indicates that at least a small quantity of the rubber phase must be present

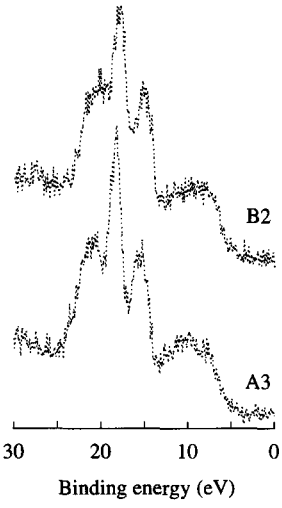

Figure 7 VB-X.p.s. spectra acquired at $\phi = 45°$. The spectra are shifted vertically. No correction for surface charging was made, which results in the peak positions being located *ca.* 2.5 eV too high

even in the topmost 10 nm of the TPOs. Apart from this observation, only minor differences were observed among the materials, from which no further conclusions could be drawn.

Characterization of the plasma-modified materials

Water contact angle measurements. The effect of oxygen plasma treatments on wettability is shown in *Tables 4* (PPs) and *5* (TPOs). The tables also include the water contact angles of the untreated materials. *Table 4* shows that similar advancing contact angles are obtained for all P/G ratios up to 2.5, after which a decrease is observed. The same trend is observed in the receding contact angles, but the decrease is in this case already discernible at P/G = 2.5. The only difference found when comparing the materials is that the A4 material generally exhibits lower contact angles than do the other materials. Again, this effect is most pronounced in the receding contact angles. *Table 5* shows that the advancing contact angles obtained for the TPOs decrease at P/G ratios higher than 2.5. The receding contact angles are also more or less constant up to P/G = 2.5, although some TPOs (e.g. B3 and B5) already show a decrease at this treatment condition. Comparing the various TPOs, it appears that B1 (containing the randomly ethylene-modified PP) and the materials with the lowest ethylene content, B3 and B5 (i.e. the three materials based on matrices that were not block ethylene-modified), demonstrate higher contact angles than the other TPOs.

Table 4 Water contact angles (advancing, θ_A; receding, θ_R) for untreated and plasma-treated PPs (A1–A4)

			P/G ratio							
	Untreated		0.25		1.0		2.5		8.0	
Material	θ_A	θ_R	θ_A	θ_R	θ_A	θ_R	θ_A	θ_R	θ_A	θ_R
A1	94	87	75	29	77	34	75	33	68	7
A2	100	95	76	32	77	30	76	26	70	11
A3	102	94	74	29	77	28	76	23	71	11
A4	98	91	71	26	73	24	73	16	61	8

Table 5 Water contact angles (advancing, θ_A; receding, θ_R) for untreated and plasma-treated TPOs (B1–B6)

			P/G ratio							
	Untreated		0.25		2.5		10		20	
Material	θ_A	θ_R	θ_A	θ_R	θ_A	θ_R	θ_A	θ_R	θ_A	θ_R
B1	101	95	77	33	74	27	68	7	63	6
B2	103	95	62	17	63	18	56	9	49	5
B3	99	94	80	32	79	25	73	9	71	8
B4	103	94	65	22	69	21	63	10	51	5
B5	97	93	81	33	79	26	71	10	69	9
B6[1]	100	94	70	26	70	23	62	6	52	5
B6[2]	101	89	68	16	67	14	58	5	51	5

Atomic composition as measured by X.p.s. X.p.s. analysis was carried out on untreated samples and samples plasma-treated at the lowest and highest P/G ratios. The results are summarized in *Tables 6* (PPs) and *7* (TPOs). In accordance with the contact angles shown in *Table 4*, all PPs reveal a higher level of oxidation after plasma treatment at P/G = 8.0 than after plasma treatment at P/G = 0.25. As regards the oxygen content, no significant variation can be observed as a result of material composition, neither at P/G = 0.25 nor at P/G = 8.0. On the other hand, the nitrogen content increases as the ethylene content in the bulk materials increases. The same trend can be observed for both P/G ratios and, although nitrogen may be incorporated into the surface at the moment the plasma-treated sample is exposed to air, or be present at the surface as a result of migration of nitrogen-containing stabilizers, it is unclear why this trend is present.

Table 7 summarizes the atomic compositions obtained for the TPOs. The table reveals that the variation in oxygen content after plasma treatment is generally greater for the TPOs than for the PPs. This may not be too surprising, keeping in mind that TPOs are more complex materials than PPs. It can also be seen that the oxygen content is higher after plasma treatment at P/G = 20 than after plasma treatment at P/G = 0.25. Furthermore, it can be noted that the materials based on the diene-modified PP (B3 and B5) are considerably less oxidized after plasma treatment at P/G = 20 than are the other TPOs. At this point, it is interesting to refer to a paper concerning corona treatment of polyolefins by Sutherland *et al.*[17]. They observed a lower oxygen

Table 6 Atomic composition of untreated and plasma-treated PPs as measured by X.p.s. The reported results are initial values obtained at $\phi = 45°$

Treatment conditons	Material	At% C	At% O	At% N
Untreated	A1	98.0	2.0	0.0
	A2	99.8	0.2	0.0
	A3	98.9	0.7	0.4
	A4	98.5	1.5	0.0
P/G = 0.25 (W mTorr^{-1})	A1	88.5	11.5	0.0
	A2	89.4	10.3	0.3
	A3	89.3	10.1	0.6
	A4	87.6	10.9	1.5
P/G = 8.0 (W mTorr^{-1})	A1	82.9	16.5	0.6
	A2	82.0	17.5	0.5
	A3	82.4	16.5	1.1
	A4	81.5	15.6	2.9

Table 7 Atomic composition of untreated and plasma-treated TPOs as measured by X.p.s. The reported results are initial values obtained at $\phi = 45°$

Treatment conditions	Material	At% C	At% O	At% N
Untreated	B1	98.0	2.0	0.0
	B2	99.8	0.2	0.0
	B3	99.9	0.1	0.0
	B4	99.9	0.1	0.0
	B5	99.7	0.3	0.0
	$B6^1$	99.1	0.9	0.0
	$B6^2$	98.4	0.8	0.8
$P/G = 0.25$ ($W\,mTorr^{-1}$)	B1	88.5	11.5	0.0
	B2	84.1	13.5	2.4
	B3	88.8	11.0	0.2
	B4	86.6	11.2	2.2
	B5	89.1	10.3	0.6
	$B6^1$	87.4	10.7	1.9
	$B6^2$	84.9	12.9	2.2
$P/G = 20$ ($W\,mTorr^{-1}$)	B1	83.9	16.1	0.0
	B2	82.8	15.2	2.0
	B3	88.2	11.2	0.6
	B4	81.7	17.0	1.3
	B5	86.6	13.4	0.0
	$B6^1$	77.9	20.2	1.9
	$B6^2$	80.1	17.8	2.1

content on a PP sample than on a corresponding PE sample after corona treatment, regardless of treatment levels. The behaviour was explained as being the result of chain scission reactions, which produce volatile low molecular weight oxidized fragments. As PP is more prone to chain scission than PE[18,19], a greater loss of oxygen is observed in the former case. Similar results and conclusions are also reported by Papirer *et al.*[20], although, in that case, the PP and PE samples were subjected to flame treatment. Indeed, the same course of events can be used to explain why, in our case, B3 and B5 reveal considerably lower oxygen contents than the others after plasma treatment at $P/G = 20$, as these are the only materials that are based on a non-ethylene-modified PP matrix. However, although the contact angles also indicated a difference between B1 and the materials based on the block ethylene-modified PP (the former revealed higher contact angles, as did B3 and B5), no significant difference in oxygen content seems to be present between these materials. An interesting observation is nevertheless that B2, B4 and B6 (the TPOs based on A3) reveal higher nitrogen contents than the other TPOs after plasma treatments at both $P/G = 0.25$ and $P/G = 20$. Considering the results presented in *Table 6*, it seems as though the nitrogen content increases with increasing ethylene content and presence of rubber. Since both factors affect the mobility of the samples, it appears as though the nitrogen originates from nitrogen-containing stabilizers which are attracted to the surface by the increase in surface polarity invoked by the plasma treatment.

Depth of oxidation. Apart from the X.p.s. analyses performed at $\phi = 45°$, analyses were also made (using the same samples) at 25° and 70° according to the following order: 45° (the values reported in *Tables 6* and *7*), 25°, 45°, 70° and 45°. The main objective was to identify whether the thickness of the oxidized layer varies as a result of material composition and P/G ratio. This can be done by comparing the oxygen contents obtained at different take-off angles. Moreover, information on the stability of the oxidized layer can also be gained by following how the oxygen content varies with X-ray exposure time (comparison of all oxygen contents obtained at 45°). Indeed, a decrease in the oxygen content was found with increasing exposure time (the decrease was *ca.* 20% after 25 min of X-ray exposure), indicating that the samples were affected by the X-ray radiation. A similar observation was reported by Nowak *et al.*[21], who detected a serious drop in the O/C ratio for an oxygen plasma-treated PP under prolonged X-ray exposure. The analyses made at different take-off angles (these were made consecutively within 15 min of X-ray exposure) revealed that the oxygen content is more or less independent of the take-off angle (apart from the small decrease caused by the X-ray radiation) for all samples treated at $P/G = 0.25$. As regards the higher P/G ratio, neither the PPs nor the major part of the TPOs (B1–B3, B5) showed any dependence on take-off angle. Consequently, the only conclusion that can be drawn for these samples is that they must have oxidized layers thicker than 10 nm. This can be compared with the results of Strobel *et al.*[22], who reported the oxidized layer to be *ca.* 10 nm after corona and remote air plasma treatments, 2–5 nm after flame treatment, while the oxidized layer after treatment in a mixture of air and ozone in combination with ultraviolet light resulted in a considerably thicker layer (in the range of 10 nm–1 μm). Although no dependence on take-off angle was observed for most of the samples treated at $P/G = 20$, a clear decrease in the oxygen content is seen for $B6^1$ and $B6^2$, and an even more pronounced decrease is observed for B4, see *Figure 8*. This reduction in oxygen content is far too large to be an X-ray-induced damage, and the oxidized layer is obviously significantly more shallow for these samples than for the rest of the samples. At present, no factor has been found that can fully explain why these particular samples should have a thinner oxidized layer, but it could be a result of different gradients in the material composition within the first 0–50 nm of the samples.

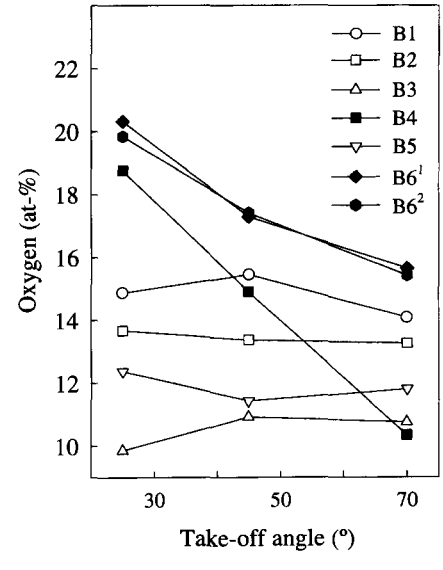

Figure 8. Oxygen content vs X.p.s. take-off angle after plasma treatment at $P/G = 20$

CONCLUSIONS

The most important findings observed during this work can be summarized as follows:

(a) The s.e.c. results revealed only minor differences among the materials, while the d.s.c. and *FT*i.r. experiments confirmed that the differences are to be expected as a result of the variation in material composition.
(b) All materials showed a gradient in material composition as measured by *FT*i.r.–ATR. The samples were generally more PP-rich at the outermost surface, and a greater extent of the ethylene-modified material and/or rubber was found at ~800 nm than at ~200 nm. Furthermore, most of the samples showed a lower degree of surface crystallinity in the topmost ~200 nm than in the first ~800 nm, and a higher mould temperature led to a higher degree of crystallinity.
(c) The water contact angles and the oxygen content were little affected by P/G ratios up to 2.5. At higher ratios, all samples were more oxidized. Moreover, at P/G = 0.25, only minor differences in water contact angles and oxygen content were observed as a result of the material composition. At higher P/G ratios, the differences were more pronounced, the materials with the lowest ethylene content being less oxidized.
(d) X.p.s. analysis revealed that the thickness of the oxidized layer was for most samples greater than 10 nm. However, B4, $B6^1$ and $B6^2$ showed significantly thinner oxidized layers than the other TPOs after plasma treatment at P/G = 20.

ACKNOWLEDGEMENTS

The authors gratefully acknowledge Borealis for financial support and for contributing the materials. The support of Volvo and Beckers Industries is also acknowledged, as are Ms Hélène Blixt and Ms Maria Ågren for their assistance with the experiments.

REFERENCES

1. Sutherland, I., Hall, D. K., Brewis, D. M., Heath, R. J., Grassmeder, J. and Waddington, S., *The Adhesion Society, Proceedings of the 16th Annual Meeting*, pp. 402–403, Williamsburg, Feb. 1993.
2. Boenig, H. V. (ed.), *Fundamentals of Plasma Chemistry and Technology. Technomic Publishing Company, Lancaster, 1988.*
3. Holländer, A., Klemberg-Sapieha, J. E. and Wertheimer, M. R., *Macromolecules* 1994, **27**, 2893.
4. Nihlstrand, A., Hjertberg, T., Schreiber, H. P. and Klemberg-Sapieha J. E., *J. Adhesion Sci. Technol.*, 1996, **10**, 651.
5. Nihlstrand, A., Hjertberg, T. and Johansson, K. S., *J. Adhesion Sci. Technol.*, accepted.
6. Flamm, D. L., in *Plasma–Surface Interactions and Processing of Materials*, ed. Auciello, O. Kluwer Academic Publishers, Dordrecht, 1990, pp. 38–44.
7. Nihlstrand, A., Hjertberg, T. and Johansson, K. S., *Polymer*, 1997, **38**, 3591.
8. Wunderlich, B., *Macromolecular Physics*, Vol. 3, p. 63. Academic Press, New York, 1980.
9. Griffiths, P. R. and de Haseth, J. A., in *Chemical Analysis*, Vol. 83 (Fourier Transform Infrared Spectrometry), ed. P. J. Elving and J. D. Winefordner. John Wiley & Sons, New York, 1986, pp. 191–194.
10. Knutson, K. and Lyman, D. J., in *Surface and Interfacial Aspects of Biomedical Polymers*, ed. J. D. Andrade. Plenum Press, New York, 1985, Vol. 1, pp. 197–247.
11. Andrade, J. D. (ed.), *Surface and Interfacial Aspects of Biomedical Polymers*. Plenum Press, New York, 1985, Vol. 1, pp. 175–184.
12. Coltrup, N. B., *Introduction to Infrared and Raman Spectroscopy*. Academic Press, New York, 1975, pp. 220–233.
13. Karger-Kocsis (ed.), *Polypropylene Structure, Blends and Composites*. Chapman & Hall, London, 1995, Vol. 1, pp. 19–21.
14. Bonnerup, C. and Gatenholm, P., *J. Polymer Sci., Polymer Physics*, 1993, **31**, 1487.
15. Pouchert, C. J., *The Aldrich Library of FT*-i.r. *Spectra*, 1st edn. Aldrich Chemical Company Inc., 1985, Vol. 1, pp. 1157–1158.
16. Beamson, G. and Briggs, D., *High Resolution XPS of Organic Polymers*. John Wiley & Sons, New York, 1992, pp. 54–57.
17. Sutherland, I., Popat, R. P., Brewis, D. M. and Calder, R., *J. Adhesion* 1994, **46**, 79
18. Mark, H. F., Bikales, N. M., Overberger, C. G. and Menges, G., *Encyclopedia of Polymer Science and Engineering*, Vol. 4, 2nd edn. John Wiley & Sons, New York, 1986, pp. 418–436.
19. Lazár, M., Rado, R. and Rychlý, J., *Adv. Polym. Sci.* 1990, **95**, 149.
20. Papirer, E., Wu, D. Y. and Schultz, J., *J. Adhesion Sci. Technol.* 1993, **7**, 343.
21. Nowak, S., Haerri, H.-P., Schlapbach L. and Vogt, J., *Surf. Inter. Anal.*, 1990, **16**, 418.
22. Strobel, M., Walzak, M. J., Hill, J. M., Lin, A., Karbashewski, E. and Lyons, C. S., *J. Adhesion Sci. Technol.*, 1995, **9**, 365.